Effect of Electron-Electron Scattering on the Carrier Distribution in Semiconductor Devices

Hans Kosina and Markus Kampl
Institute for Microelectronics, Technial University Wien, Vienna, Austria

I. Introduction

It is commonly accepted that electron-electron scattering (EES) alters the high-energy tail of the energy distribution function [1] [2], and thus plays an important role in the physically-based modeling of hot carrier degradation [3]. One can distinguish between selfconsistent models which assume the actual or an approximate non-equilibrium distribution for the partner electrons, and non-selfconsistent models which assume an equilibrium distribution for the partner electrons. The latter approach is suitable to describe the interaction of channel hot electrons with a reservoir of cold electrons in the drain region. This case is studied in the present work. We briefly discuss the details about the derivation of the single-particle scattering rate and the implementation in a Monte Carlo simulator for both parabolic bands and full-band structures.

II. Theory

The two-particle transition rate for binary collisions of two electrons is given by Fermi's Golden rule.

$$P_2(\boldsymbol{k}_1,\boldsymbol{k}_2;\boldsymbol{k}_1',\boldsymbol{k}_2') = \frac{2\pi}{\hbar}\left|\langle \boldsymbol{k}_1',\boldsymbol{k}_2'|V|\boldsymbol{k}_1,\boldsymbol{k}_2\rangle\right|^2 \times \delta\big[\epsilon(\boldsymbol{k}_1')+\epsilon(\boldsymbol{k}_2')-\epsilon(\boldsymbol{k}_1)-\epsilon(\boldsymbol{k}_2)\big] \quad (1)$$

Assuming screened Coulomb interaction and plane waves for the electronic states gives the following matrix element [4], [5]:

$$\langle \boldsymbol{k}_1',\boldsymbol{k}_2'|V|\boldsymbol{k}_1,\boldsymbol{k}_2\rangle = \left(\frac{e^2}{\epsilon_s\Omega}\right)\frac{\delta_{\boldsymbol{k}_1+\boldsymbol{k}_2,\boldsymbol{k}_1'+\boldsymbol{k}_2'}}{\left|\boldsymbol{k}_1-\boldsymbol{k}_1'\right|^2+\beta_s^2} \quad (2)$$

The transition rate (1) is symmetric.

$$P_2(\boldsymbol{k}_1,\boldsymbol{k}_2;\boldsymbol{k}_1',\boldsymbol{k}_2') = P_2(\boldsymbol{k}_1',\boldsymbol{k}_2';\boldsymbol{k}_1,\boldsymbol{k}_2) \quad (3)$$

This property is in accordance with the principle of detailed balance for energy-conserving transitions.

In order to include EES in the single-particle framework of the Boltzmann equation, one has to reduce the two-particle scattering rate to a single-particle scattering rate. This, of course, cannot go without approximations. To describe the mixing of hot electrons from the channel with cold electrons in the drain, it is reasonable to assume a Fermi-Dirac distribution for the drain electrons. The single-particle transition rate for the sample electron is obtained by summing over all initial states $\boldsymbol{k}_2$ and final states $\boldsymbol{k}_2'$ of the partner electrons. The factor 2 accounts for spin-degeneracy of the $\boldsymbol{k}_2$ states.

$$P_1(\boldsymbol{k}_1,\boldsymbol{k}_1') = \sum_{\boldsymbol{k}_2,\boldsymbol{k}_2'} P_2(\boldsymbol{k}_1,\boldsymbol{k}_2;\boldsymbol{k}_1',\boldsymbol{k}_2') \times 2f_0(\boldsymbol{k}_2)\left[1-f_0(\boldsymbol{k}_2')\right] \quad (4)$$

Using this definition of P_1, the symmetry property (3), and the Fermi-Dirac distribution f_0, the following relation can be proved.

$$P_1(\boldsymbol{k}_1',\boldsymbol{k}_1) = P_1(\boldsymbol{k}_1,\boldsymbol{k}_1')\,\mathrm{e}^{[\epsilon(\boldsymbol{k}_1')-\epsilon(\boldsymbol{k}_1)]/k_BT} \quad (5)$$

In the single-particle picture the transitions are inelastic and the transition rate satisfies the principle of detailed balance. In the context of device simulation, this means that EES will establish a Maxwellian high-energy tail, provided that interaction with an equilibrium electron system is considered. Note that (5) holds true for arbitrary dispersion relations $\epsilon(\boldsymbol{k})$.

III. Implementation

One out of the two sums in (4) can be readily evaluated by means of the Kronecker-delta in (2), which imposes momentum conservation. The second sum is converted to an integral. The latter can be solved analytically under the following assumptions regarding the partner electrons: i) $f_0(\boldsymbol{k}_2)$ is a Maxwell-Boltzmann (MB) or Fermi-Dirac (FD) distribution, and ii) the energy dispersion $\epsilon(\boldsymbol{k}_2)$ is parabolic. For the sake of brevity we only show the result for a MB distribution:

$$S_1(\boldsymbol{k}_1,\boldsymbol{k}_1') = \frac{\Omega}{(2\pi)^3}P_1(\boldsymbol{k}_1,\boldsymbol{k}_1') = \frac{ne^4}{(2\pi)^{3/2}\hbar^2\epsilon_s^2}\sqrt{\frac{m}{k_BT}}\,\frac{1}{q\left(q^2+\beta_s^2\right)^2} \times \exp\left(-\frac{\left(\epsilon(\boldsymbol{k}_1')-\epsilon(\boldsymbol{k}_1)+E_q\right)^2}{4k_BTE_q}\right) \quad (6)$$

with

$$q = \left|\boldsymbol{k}_1'-\boldsymbol{k}_1\right|, \qquad E_q = \frac{\hbar^2\left|\boldsymbol{k}_1'-\boldsymbol{k}_1\right|^2}{2m}$$

The total scattering rate Γ_1 is obtained from (6) by integration over the final states of the sample electron:

$$\Gamma_1(\boldsymbol{k}_1) = \int S(\boldsymbol{k}_1,\boldsymbol{k}_1')\,\mathrm{d}^3k_1' \quad (7)$$

978-1-5386-6790-3/18/$31.00 ©2018 IEEE

Up to this point, no assumption about $\epsilon(\boldsymbol{k}_1)$, the dispersion relation of the sample electron, has been made. This fact allows us to construct a model in which the a (high-energetic) sample electron in a fullband structure is interacting with a (low-energetic) partner electron in a parabolic valley. This model is applicable if the distribution of the partner electrons remains close to equilibrium. The integral in (7) is approximated by a discrete sum in $\boldsymbol{k}$-space. To facilitate the selection of the after-scattering state, all partial sums of the form

$$\Gamma_1(\boldsymbol{k}_n, N) \approx \sum_{\boldsymbol{k}_m}^{N} S(\boldsymbol{k}_n, \boldsymbol{k}_m; b, E_F)\, V_m, \qquad N = 1, 2, \ldots N_n \quad (8)$$

are pre-computed and stored in a table. Here, $\boldsymbol{k}_n$ and V_n denote the center and the volume of the n-th tetrahedron, respectively. The sum includes all tetrahedra m in the neighborhood of tetrahedron n whose contributions to the sum are greater than a predefined tolerance. If the number of tetrahedra satisfying this criterion is denoted by N_n, the total scattering rate equals $\Gamma_1(\boldsymbol{k}_n, N_n)$. A table of partial sums (8) is stored for each discrete initial state $\boldsymbol{k}_n$ in the irreducible wedge of the Brillouin zone, for each band b, and for a set of discrete Fermi levels E_F in the case of Fermi-Dirac statistics. The final state is obtained by randomly selecting a tetrahedron $m \in [1, N_n]$ using the pre-computed table of partial sums.

The next model we want to discuss assumes a parabolic dispersion for both the sample and the partner electron, which, of course, is the standard model often used in literature. From (6) a scattering rate of the following form can be derived:

$$\Gamma_1(\epsilon) = \frac{e^2\sqrt{m k_B T}}{(2\pi)^{3/2}\hbar^2\epsilon_s} F\left(\sqrt{\epsilon/k_B T}, \hbar\beta_s/\sqrt{2mk_B T}\right) \quad (9)$$

The function F defined in the following is evaluated by means of numerical integration.

$$F(p, x) = \int_0^\infty \frac{s^2}{s^2 + x^2} \frac{\mathrm{e}^{-(s-p)^2} - \mathrm{e}^{-(s+p)^2}}{2p}\, \mathrm{d}s\,. \quad (10)$$

Since ionized-impurity scattering (IIS) and e-e scattering (EES) are caused by the very same screened Coulomb interaction, we compare the rates of these two scattering mechanisms in Fig. 1 and Fig. 2. In both cases, the scattering rate becomes smaller with increasing concentration. However, since the scattering potential gets more localized with stronger screening, its distribution in momentum space gets wider, and hence the momentum transferred per scattering event gets larger. At high energies, the rates become concentration-independent in both cases. The main differences can be observed at low energies. While an electron at rest is strongly affected by the moving partner electrons, it will not be affected by the static impurities. At low energies, the EES rate assumes a constant value determined by $F(0, x)$, whereas the IIS rate vanishes for a non-zero screening parameter β_s. For weak screening ($\beta_s \to 0$) the EES rate converges to a finite value determined by $F(0, 0) = 1$, whereas the maximum of the IIS rate grows indefinitely, see Fig. 2.

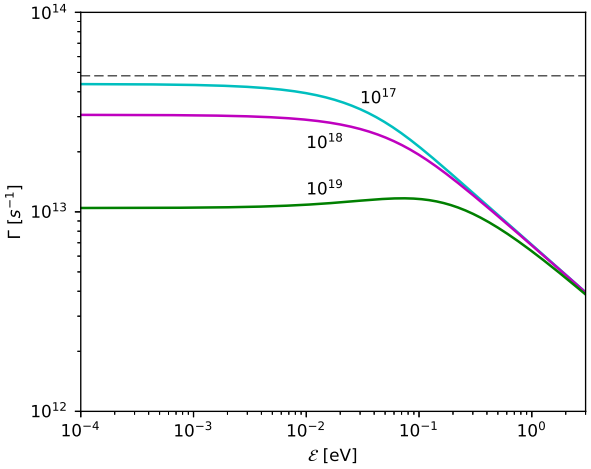

Fig. 1. Electron-electron scattering rate calculated from (9) assuming $m = 0.3m_0$, $\epsilon_s = 11.68\epsilon_0$ and $T = 300K$. The dashed line represents the unscreened limit of the scattering rate.

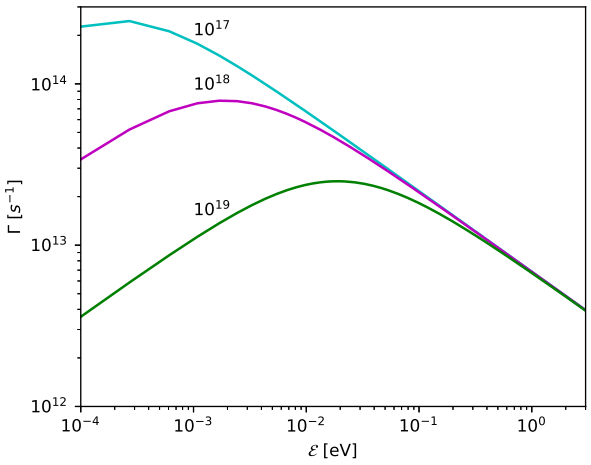

Fig. 2. Ionized-impurity scattering rate obtained from the Brooks-Herring model [6] for the same parameters as in Fig. 1.

IV. Results for Bulk Silicon

In a first test, the equilibrium distribution function is simulated. Assuming a parabolic dispersion in the simulation, consistent with the integration of the transition rate (6), gives an equilibrium Maxwellian also in the presence of EES. This is expected since EES satisfies the principle of detailed balance. The numbers of energy gain and loss processes are perfectly balanced for each

scattering mechanism. Using the transition rate (6) in a MC simulation with a non-parabolic dispersion ($\alpha = 0.5\,\mathrm{eV}^{-1}$), however, results in an imbalance of energy gain and loss processes. An excess of phonon emissions over absorptions indicates that the inconsistently used EES model provides net energy to the electron system.

This example indicates that analytical formulae derived for a parabolic dispersion should not be used in a transport model with any other band-structure.

V. Results for Silicon Devices

The EES model has been implemented in the Monte Carlo device simulator VMC [7] for both analytical and numerical band structures. The first device investigated is an $n^+n^-n^+$ diode with abrupt junctions. The doping levels are $10^{19}\mathrm{cm}^{-3}$ and $10^{15}\mathrm{cm}^{-3}$, respectively. Fig. 3 shows the conduction band edge for an applied voltage of 2 V and the electron densities. The plot distinguishes between the total electron density and the density of electrons originating from the source contact only. Cooling of the hot carriers in the drain region is discussed in Fig. 4.

The second device we consider is a planar n-channel MOSFET with $L_G = 65\,\mathrm{nm}$, $t_{\mathrm{ox}} = 2.5\,\mathrm{nm}$, and a channel width of $W = 1\,\mu\mathrm{m}$. Device geometry and doping profiles have been obtained by process simulation [8]. The first simulation assumes a parabolic band. Fig. 5 shows the EDF at three surface points in the channel at $V_{GS} = 2.2\,\mathrm{V}$ and $V_{DS} = 2.2\,\mathrm{V}$. Fig. 5 indicates that EES has virtually no influence on the non-equilibrium EDF. The reason is that the EES transition rate (6) satisfies the principle of detailed balance and thus does not alter the Maxwellian high energy tail.

The full-band implementation of the EES model in the MC code requires a numerical integration over the Brillouin zone. Fermi-Dirac statistics for the initial state and the Pauli blocking factor for the final state of the partner electron are taken into account. The after-scattering state is selected randomly using pre-calculated lists of tetrahedra. To resolve the high energy tail accurately, we employ the recently developed backward MC method [9] [10].

In Fig. 6 results from full-band transport calculations are compared to the results of ViennaSHE, a deterministic solver for the BE based on a spherical harmonics expansion of the distribution function [11]. That simula-

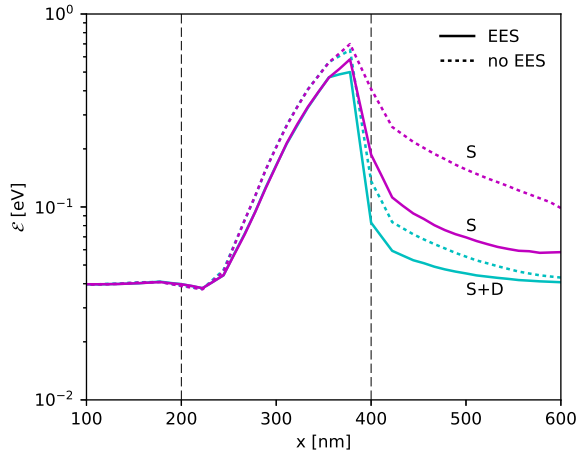

Fig. 4. Average electron energy in the $n^+n^-n^+$ diode. The upper curves (S) consider only the (hot) electrons originating from the source region and clearly show the additional energy relaxation due to EES. The lower curves (S+D) consider all electrons and show a stronger carrier cooling because in addition to energy relaxation there occurs also a mixing of the hot carriers with the cold carriers in the drain.

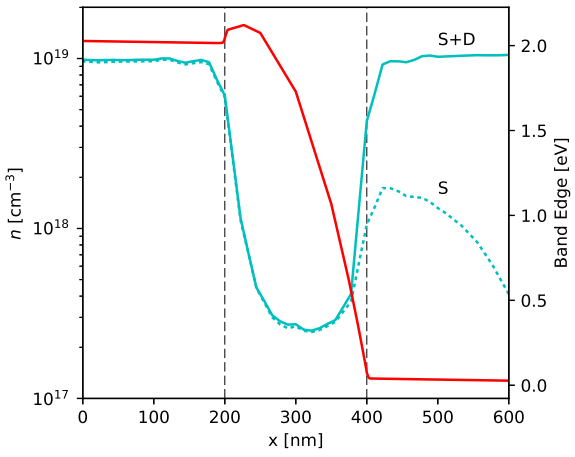

Fig. 3. Conduction band edge in an $n^+n^-n^+$ diode with abrupt junctions. The total electron density (S+D) and the partial density due to electrons injected from the source contact (S) are shown.

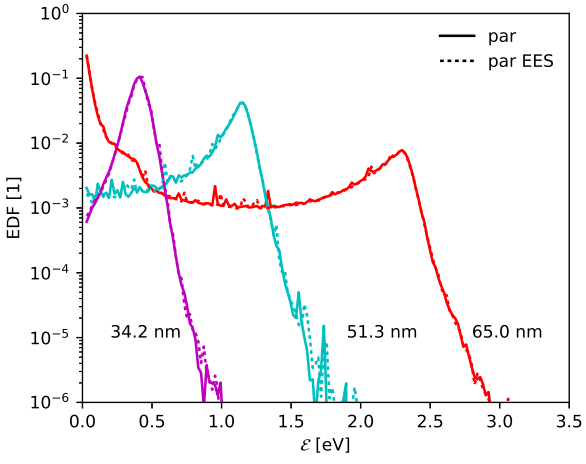

Fig. 5. EDF at three surface points in the channel of a MOSFET with and without EES. A parabolic dispersion is assumed in the transport model to be consistent with the EES-rate (9).

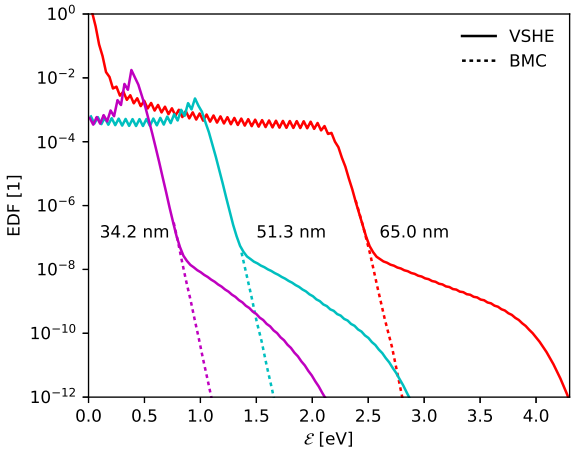

Fig. 6. EDF at three surface points in the channel with EES and fullband effects included. The backward MC simulation accounts for interaction with cold drain electrons and predicts a Maxwellian tail (dashed line). ViennaSHE considers interaction with non-equilibrium electrons at a fixed energy and severely overestimates the high-energy tail.

tor accounts for an isotropic, multi-valley band-structure that captures some features of the full-band density of states. In the EES model, additional approximations are introduced. For instance, the energy of the partner electron before scattering is treated as a constant (ϵ^*) which is set equal to the average energy. As shown in Fig. 6, the MC model predicts a Maxwellian tail at high energies in accordance with the assumption that the hot carriers interact with an equilibrium system of cold carriers, whereas the EES model of ViennaSHE predicts a significant deviation from the Maxwellian tail. We believe that an EES model that properly fulfills energy and momentum conservation simultaneously would not be able to yield such strong enhancements of the high energy tail as reported in [1] [8] and [12].

VI. Summary

Theoretical properties of the EES scattering rate and the reduction to a one-particle model are briefly discussed. In contrast to the divergence of the ionized-impurity scattering rate in the unscreened limit, the EES rate is convergent.

A model for electron-electron scattering is proposed, which consistently combines a full-band structure for the sample electron with a parabolic dispersion for the partner electrons. By assuming an equilibrium distribution for the latter, the model is able to describe the mixing of hot carriers with a reservoir of cold carriers. This model gives an upper estimate for the effect of EES since heating of the partner electrons is neglected and thus the difference of the mean energies of the hot and cold ensembles is bigger than it would be in a self-consistent model.

Acknowledgement

This work was supported by the Austrian Research Promotion Agency (FFG), project MORAFLASH (contract No. 850660). The computational results presented have been achieved in part using the Vienna Scientific Cluster (VSC).

References

[1] P. A. Childs and C. C. C. Leung, "A one-dimensional solution of the Boltzmann transport equation including electron-electron interactions," *Journal of Applied Physics*, vol. 79, p. 222, 1996.

[2] C. C. C. L. M. Y. Chang, D. W. Dyke and P. A. Childs, "High-energy electronelectron interactions in silicon and their effect on hot carrier energy distributions," *Journal of Applied Physics*, vol. 82, p. 2974, 1997.

[3] S. E. Rauch, G. L. Rosa, and F. J. Guarin, "Role of e-e scattering in the enhancement of channel hot carrier degradation of deep-submicron NMOSFETs at high v_{GS} conditions," *IEEE Transactions on Device and Materials Reliability*, vol. 1, no. 2, pp. 113–119, 2001.

[4] K. Tomizawa, *Numerical Simulation of Submicron Semiconductor Devices*. Artech House, 1993.

[5] B. Ridely, *Quantum Processes in Semiconductors*. Oxford University Press, 2013.

[6] C. Jacoboni and P. Lugli, *The Monte Carlo Method for Semiconductor Device Simulation*. Wien-New York: Springer, 1989.

[7] *VMC Homepage* . [Online]. Available: http://www.iue.tuwien.ac.at/index.php?id=vmc

[8] S. E. Tyaginov, M. Bina, J. Franco, D. Osintsev, O. Triebl, B. Kaczer, and T. Grasser, "Physical Modeling of Hot-Carrier Degradation for Short- and Long-channel MOSFETs," in *Conference Proceedings of International Reliability Physics Symposium*, 2014, pp. XT16.1 – XT16.8.

[9] M. Kampl and H. Kosina, "Investigation of Hot-carrier Effects Using a Backward Monte Carlo Method and Full Bands," in *Conference Proceedings of International Workshop on Computational Nanotechnology*, 2017, pp. 147 – 148.

[10] ——, "Hot Carrier Study Including e-e Scattering Based on a Backward Monte Carlo Method," in *Proceedings of the 22nd International Conference on Simulation of Semiconductor Processes and Devices*, 2017, pp. 293 – 296.

[11] *ViennaSHE User Manual*, 2018. [Online]. Available: http://viennashe.sourceforge.net/doc/

[12] M. Bina, S. Tyaginov, J. Franco, K. Rupp, Y. Wimmer, D. Osintsev, B. Kaczer, and T. Grasser, "Predictive hot-carrier modeling of n-channel MOSFETs," *IEEE Transactions on Electron Devices*, vol. 61, no. 9, pp. 3103–3110, 2014.